JOC The Journal of Organic Chemistry

Article

pubs.acs.org/joc

A Theoretical Mechanistic Study of the Asymmetric Desymmetrization of a Cyclic *meso*-Anhydride by a Bifunctional Quinine Sulfonamide Organocatalyst

Katie Blise, Milan W. Cvitkovic, Nolly J. Gibbs, Sean F. Roberts, Reid M. Whitaker, Gretchen E. Hofmeister,* and Daniela Kohen*

Department of Chemistry, Carleton College, Northfield, Minnesota 55057, United States

Supporting Information

ABSTRACT: Cinchona alkaloids and their derivatives are widely used as organocatalysts in asymmetric synthesis. In particular, sulfonamide derivatives of cinchona alkaloids are highly enantioselective desymmetrization catalysts in the ring opening of a variety of cyclic anhydrides. To better understand the mechanism of catalysis, as well as to identify the basis for enantioselectivity by this catalyst, we have performed DFT calculations of this reaction with a cyclic *meso* anhydride. Herein, we report calculations for two reaction pathways, one concerted and one stepwise, for the production of each enantiomer of the desymmetrized product using the complete sulfonamide catalyst **I**. Our results are consistent with both the enantioselectivity of this transformation and the catalytic role of the quinuclidine moiety. We find that the stepwise pathway is the relevant pathway in the production of the major enantiomer. Our calculations highlight the role of differential distortion of the anhydride−methanol complex in the transition state as the factor leading to stereoselectivity.

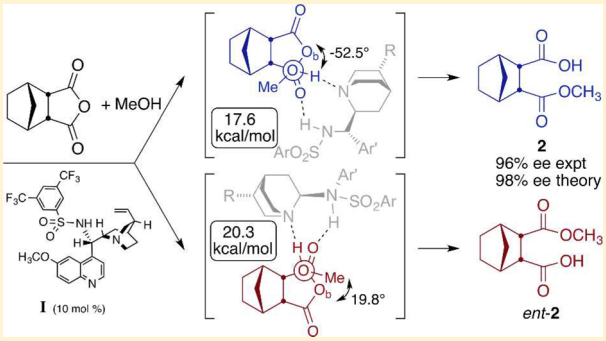

INTRODUCTION

The organocatalytic asymmetric desymmetrization (ASD) of *meso* or achiral cyclic anhydrides with methanol introduces chirality into inexpensive achiral feedstock[1−5] and has been applied in the total synthesis of biologically active compounds.[5−11] A variety of effective organocatalysts have been developed for this ASD reaction, but those based on cinchona alkaloids are the most frequently used. In addition to the native alkaloids, several ether[12] and 9-amino(9-deoxo)*epi* derivatives have been studied. This latter class of catalysts can incorporate thiourea,[13−16] squaramide,[17,18] or sulfonamide[19,20] hydrogen bond donating groups in addition to the quinuclidine functional group of the native alkaloid. Of these, sulfonamides (e.g., **I**, eq 1) developed by Song, Chin and co-workers in 2008,[19] are top performers because they provide excellent enantiomeric excess at room temperature for a wide range of substrates (ee = 91−98%)[19,21] and they are not susceptible to erosion of ee due to homodimerization.[18] These catalysts have also been employed in enantioselective conjugate additions.[22−24]

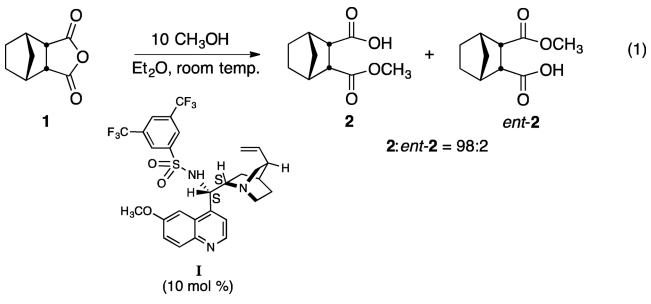

(1)

Song et al. introduced the hydrogen bond donating groups with the purpose of activating the anhydride electrophile in addition to the methanol nucleophile. To support this bifunctional activation model, they presented computational studies of the ASD using anhydride substrates that were also studied experimentally. To the best of our knowledge, this is the only previously published computational study of catalyst **I**.[19,25] To find the relevant complexes, the authors identified enantiomeric zwitterionic species resulting from the interaction of anhydride and methanol. Using molecular mechanics, they performed global minimum-energy searches of each zwitterionic species interacting with **I**. The relative energies of the resultant complexes were then calculated using B3LYP at the 6-31G* level in the gas phase. Two sites of interaction between the species leading to the major enantiomer and the catalyst were identified: (i) the quinuclidine nitrogen, which accepts a hydrogen bond from the methanol group, and (ii) the sulfonamide proton, which stabilizes the oxyanionic group of

Received: September 21, 2016
Published: December 13, 2016

DOI: 10.1021/acs.joc.6b02320
J. Org. Chem. 2017, 82, 1347−1355

the zwitterionic species by acting as a hydrogen bond donor (Figure 1). The calculated differences in energy between

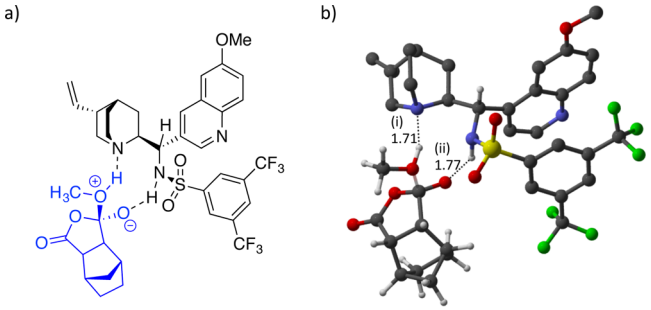

Figure 1. (a) Catalyst–zwitterionic complex leading to the major enantiomer proposed by Song et al. (b) Calculated catalyst–zwitterionic complex, with distances (i) quinuclidine···HOMe and (ii) sulfonamide H···O═C in Å.[19]

complexes of **I** with each of the enantiomeric zwitterions produce reasonable agreement with the experimental ees.[26] However, their results indicated that the zwitterionic species leading to the minor enantiomer does not hydrogen bond with the quinuclidine nitrogen; this contradicts the expectation that the quinuclidine moiety acts as a general base in these reactions, regardless of the enantiomer produced.

The generally accepted mechanism of catalysis by cinchona alkaloids in this ASD reaction is general base activation of the methanol nucleophile by the quinuclidine nitrogen.[1,2] Early reports using native alkaloids (e.g., **II**, Figure 2) identified the

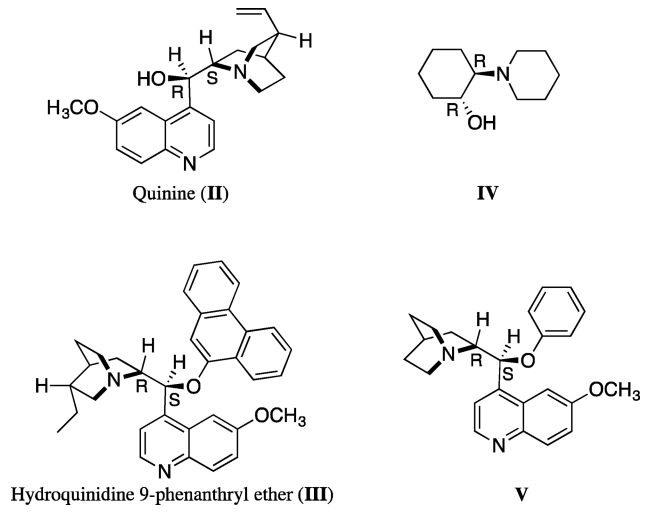

Figure 2. Other catalysts studied experimentally (**II**,[27,29,34] **III**,[12] **IV**[16]) and computationally (**II**,[35,36] **IV**,[33] **V**[37]) in this asymmetric desymmetrization reaction.

quinuclidine group as that responsible for catalysis.[27−29] Two possible roles can be envisioned for the quinuclidine in the rate-limiting step: nucleophilic activation of the anhydride or general base activation of the methanol. Although there is some evidence in favor of nucleophilic activation,[30] kinetic studies are more consistent with the general base activation model. Oda and co-workers found a first-order rate dependence on methanol and a primary isotope effect for $^{1}HOCH_3$ versus $^{2}HOCH_3$ (k_H/k_D = 2.3).[27,28] Later, Deng and co-workers applied modified cinchona alkaloids (e.g., **III**, Figure 2) as organocatalysts in this ASD transformation,[12] and in addition to a first-order rate dependence on methanol, the transformation was found to be first-order in anhydride and catalyst.[31] ROESY NMR studies by Uccello-Barretta and co-workers indicated that the catalysts used by Deng interact significantly with methanol in solution but not with the anhydride,[32] supporting a general base role for the alkaloid-based catalyst. Finally, DFT studies by Aviyente and co-workers of both the nucleophilic and the general base pathways for a related chiral *β*-hydroxy tertiary amine (**IV**, Figure 2) show that the general base pathway is favored by nearly 27 kcal/mol.[33] Overall, the data support the catalytic pathway outlined in Figure 3, in which the slow step involves stabilization of a zwitterionic species **3** (or *ent*-**3**) by the catalyst.

In the base-catalyzed mechanism, nucleophilic attack and ring opening can occur simultaneously, or the attack can occur first and then be followed by the ring opening. For example, the DFT studies by Aviyente and co-workers identified transition states (TSs) and intermediates for both the stepwise and concerted pathways for catalyst **IV**.[33] Thus, complex [**3**·catalyst] (or [*ent*-**3**·catalyst]) represents an intermediate in a stepwise mechanism and a TS in a concerted mechanism in Figure 3. Note that in the former case the ring is still closed in complex [**3**·catalyst] (or [*ent*-**3**·catalyst]), while in the latter it is partially opened.

Given the very high performance of catalyst **I**, the utility of the reactions it catalyzes, and the lack of detail in the mechanism of catalysis proposed by Song et al., we decided to perform DFT calculations of this reaction with substrate **1** (eq 1). The calculations described below allow us to improve our understanding of the chemical basis for enantioselectivity by this catalyst. Our results are in excellent agreement with the enantioselectivity of this transformation and are consistent with the catalytic role of the quinuclidine moiety.

RESULTS AND DISCUSSION

Our DFT and NMR studies of the conformational space of the catalyst **I** are presented below, followed by our mechanistic studies of the reaction in eq 1.

Catalyst Conformations. Cinchona alkaloids and their derivatives adopt several conformations at room temperature. The structures of the parent cinchona alkaloids and ether or ester derivatives thereof,[38−46] C-9 epimers of the parent alkaloids[47] and 9-thiourea(9-deoxy)*epi* derivatives of quinine and quinidine,[48,49] have been studied by solution NMR spectroscopy, X-ray crystallography, and/or by computational methods. Apart from the X-ray structure[21] and calculations[19,21] of **I** done by Song et al., and the X-ray structure of a related sulfonamide,[50] we are not aware of any previous structural studies done on 9-sulfonamide(9-deoxy)*epi* cinchona alkaloid derivatives of the type used in this work.

The NMR spectra of the quinine-derived sulfonamide **I** show two dominant conformations at room temperature, in both chloroform-d and diethyl ether-d_{10}. Analysis of dipolar couplings (NOEs) in the NMR spectra provided initial models of the two conformers, which interconvert by slow rotation about the C_9–quinoline bond (Figure 4). In addition, the $^{3}J_{H9-H8}$ coupling constant (11 Hz in both conformers) is consistent with an *anti* relationship for H_8 and H_9. This conformation about the C_8–C_9 bond is analogous to the "open" form identified for 9-*epi*-dihydroquinidine[42] and the monomeric forms of a thiourea derivative of quinine.[49] In

DOI: 10.1021/acs.joc.6b02320
J. Org. Chem. 2017, 82, 1347−1355

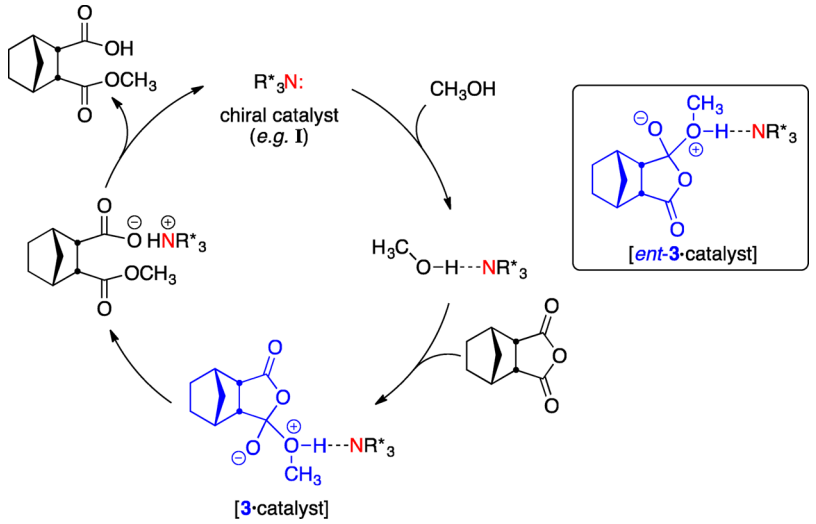

Figure 3. General base catalytic mechanism.

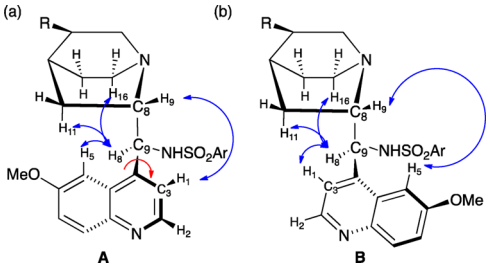

Figure 4. Schematic conformations of **I** in $CDCl_3$ and diethyl ether-d_{10} (R = vinyl, Ar = 3,5-$(CF_3)_2$Ph). Conformers are interchanged by rotation about the C_9–quinoline bond, which is indicated by a red arrow. Observed NOE crosspeaks are indicated by blue arrows.

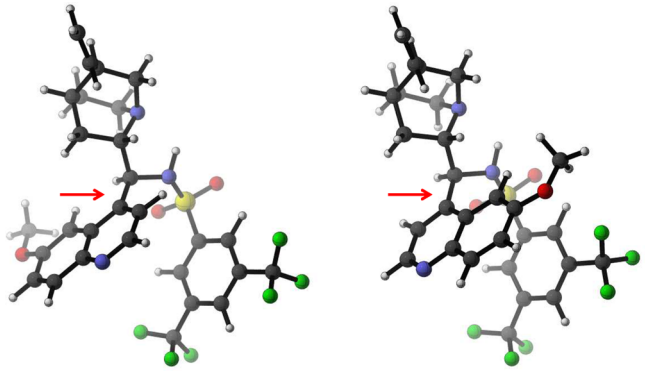

Figure 5. Calculated DFT (B3LYP/6-31G(d)/SMD/diethyl ether) structures of the two lowest energy conformers in diethyl ether solvent.

chloroform, the conformers are equally stable, whereas conformer **A** is slightly favored in diethyl ether (**A**:**B** = 60:40).

In addition to solvent effects on catalyst conformer populations, the presence of strong hydrogen bond donors favors conformer **A** over **B** in chloroform and diethyl ether. We have observed this effect with structurally different carboxylic acids, indicating that it is due to the carboxylic acid functional group. This behavior is illustrated by the NMR sample of the catalyst interacting with a product related to **2**. In this case, a 0.1 M solution of the didehydro analog of hemiester **2** combined with catalyst **I** (2:1 ratio of **2**:**I**) in $CDCl_3$ shows a conformer ratio of 81:19 (**A**:**B**) (see Supporting Information (SI)). Conformer **A** is presumably favored because the protonated quinuclidine is more accessible for ion pairing with the carboxylate anion in this conformer. Others have found comparable effects for cinchona alkaloids in the presence of carboxylic acids[51−54] or methanol.[32]

An important first step of this study was to identify the predominant catalyst conformers and evaluate them against the NMR observations. Candidate geometries were obtained by a combined approach of coordinate scans and Monte Carlo molecular mechanics. Subsequent full DFT geometry optimization using the B3LYP functional at the 6-31G(d) level of theory using SMD implicit chloroform or diethyl ether solvent yielded two predominant conformers (see Figure 5) that differ by the rotation about the C_9–quinoline bond, highlighted in both Figures 4 and 5 with a red arrow.

The calculated structures are consistent with the NOE interactions identified in Figure 4 and give H_9–C_8–C_9–H_8 dihedral angles of 176° for **A** and 174° for **B**, in accordance with the coupling constants observed in the NMR spectrum. Furthermore, the equilibrium populations predicted by the calculations in either chloroform (55:45) or diethyl ether (83:17) are also in good agreement with those determined from their NMR spectra (50:50 in $CDCl_3$ and 60:40 in Et_2O-d_{10}). Note that these equilibrium populations were obtained from free energies calculated by adding the free energy correction, obtained using a 6-31G(d) basis set, to a molecular energy determined using B3LYP-GD3BJ/6-31+G(d,p)/SMD/diethyl ether. The D3 version of Grimme's dispersion with Becke–Johnson damping (GD3BJ)[55] was applied to account for dispersion interactions.

We also examined the energies of the conformers obtained by rotation around the C_8–C_9 bond. The energy profile strongly favors an *anti* relationship for H_9 and H_8, with a rotational barrier of approximately 13 kcal/mol (see Figure S6). This strong conformational preference, also characteristic of 9-azido(9-deoxy)*epi* quinine,[56] positions the quinuclidine nitrogen and sulfonamide proton for dual activation of the reactants.

As described in the SI, the predominant conformers discussed above were also obtained using other functionals

DOI: 10.1021/acs.joc.6b02320
J. Org. Chem. 2017, 82, 1347−1355

that have been developed to accurately model dispersion interactions. We chose to proceed using B3LYP-GD3BJ/6-31+G(d,p)//B3LYP/6-31G(d) because this method not only gives meaningful results, but also others have found this approach to be a good compromise between accuracy and feasibility for modeling cinchona alkaloids and their derivatives.[37,57]

In both conformers, intramolecular aromatic stacking between the quinoline ring and the sulfonamide aromatic group plays an important role in defining the catalyst shape. The same type of π stacking is observed in the X-ray crystal structure,[21] in which the catalyst adopts conformer **A**, and it explains why NOE crosspeaks are observed between protons on the quinoline ring and the sulfonamide aryl ring in the solution NMR spectra (see SI). The net result of this aromatic attraction is that it causes the sulfonamide proton to be exposed for hydrogen bonding to other species. This *intramolecular* π-stacking is distinctive among the aromatic derivatives of cinchona alkaloids; a search of related cinchona alkaloid derivatives in the Cambridge Crystallographic Data Centre[58] did not reveal any additional examples. It is likely that this conformer also predominates in the 9-arylsulfonamido(9-deoxy)*epi* cinchona alkaloid catalyzed addition of alkyl peroxides to nitroalkenes, thereby exposing the quinuclidine nitrogen to activate the alkyl hydrogen peroxide nucleophile and the sulfonamide proton to activate the nitroalkene electrophile.[22]

The calculated structures show some pyramidalization at the sulfonamide nitrogen atom (angles H−N−C and H−N−S = 108°; angle S−N−C = 119°). This pyramidalization also occurs in Song's calculated complexes of [**3**·**I**] (or [*ent*-**3**·**I**]), but it is inconsistent with the planar nitrogen atom observed in the crystal structure. However, the crystal structure of a related sulfonamide derivative shows pyramidalization of the sulfonamide nitrogen atom, accompanied by close interactions between the sulfonamide proton and two other nitrogen atoms in the structure (2.3 Å contacts).[50] We also observe a close contact between the sulfonamide proton and the quinuclidine nitrogen (2.1 Å) in our calculated structures; that same interaction in the crystal structure of **I** is 2.9 Å.[21]

Investigation of the Reaction Mechanism. We next investigated the methanolysis mechanism of anhydride **1** in the presence of catalyst **I** in Et_2O (using SMD implicit solvent[59]). As with the catalyst conformer studies, and given the size and complexity of the system, the TS searches, geometry optimizations of the intermediate species, and frequency calculations were performed with the smaller basis set (6-31G(d)) and subsequent SP calculations were done using B3LYP-GD3BJ/6-31+G(d,p).

In order to identify stationary states, two degrees of freedom were important. A naïve understanding of the reaction suggests that the TS could be found by exploring the energy landscape as the bond length between the methanol oxygen and the carbonyl carbon changed (distance "a" in Figure 6). However, the role of the catalyst at stabilizing the TS is such that it is also crucial to scan the methanol O−H bond length (distance "b" in Figure 6) to successfully find the relevant TS.

The mechanism and outcomes shown below are those that result when catalyst **I** adopts conformation **A**. In conformer **B**, the methoxy substituent on the quinoline ring partially blocks the interaction between the methanol−anhydride complex and the quinuclidine ring. The greater accessibility of the quinuclidine nitrogen in conformer **A** is also indicated by the

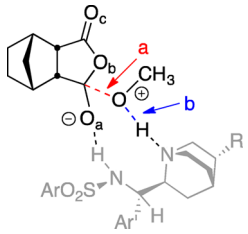

Figure 6. Important degrees of freedom for TS search: a and b. R = vinyl, Ar = 3,5-$(CF_3)_2$Ph, Ar′ = (6-methoxyquinolin-4-yl). The anhydride oxygen labeling scheme is also shown.

NMR studies of the catalyst−carboxylic acid mixtures (*vide supra*).

We identified transition states and intermediates leading to the major enantiomer via either a concerted or a stepwise reaction in ether. Figure 7 lists both the free energies calculated

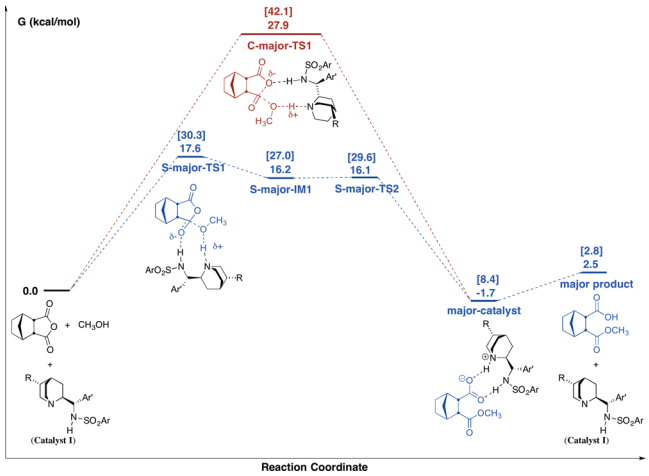

Figure 7. Concerted (red) and stepwise (blue) pathways leading to the major enantiomer. Species were minimized or optimized using B3LYP/6-31G(d) and SMD implicit diethyl ether. Thermal corrections at 1 atm and 298 K were added to their molecular energies to obtain the free energies shown in square brackets. The free energies shown without brackets were obtained using SP energies calculated using B3LYP-GD3BJ/6-31+G(d,p) also with SMD implicit diethyl ether. Energies are in kcal/mol. For catalyst **I**: R = vinyl, Ar = 3,5-$(CF_3)_2$Ph, Ar′ = (6-methoxyquinolin-4-yl).

in ether at the lower level (in square brackets), as well as those calculated at the higher level, with GD3BJ correction. These results show that the first TS is rate limiting for both the stepwise and concerted pathways. The higher level calculations result in a reasonable reaction barrier for the stepwise process. However, the concerted pathway is not a significant contributor to the major product at room temperature.

The energy surface progressing along the stepwise reaction coordinate from the first TS through the second TS is fairly flat. The transition between **S-major-TS1** and the tetrahedral intermediate (**S-major-IM1**) is exergonic, as it involves completing the transfer of the methanol OH proton to the catalyst quinuclidine nitrogen and formation of the C−OMe bond at the tetrahedral carbon. However, the calculated energies of the tetrahedral intermediate (**S-major-IM1**) and second transition state (**S-major-TS2**) at the higher level and corrected for empirical dispersion are very close, with **S-major-TS2** slightly lower in energy than **S-major-IM1**. The obvious structural differences between **S-major-IM1** and **S-major-TS2**

DOI: 10.1021/acs.joc.6b02320
J. Org. Chem. 2017, 82, 1347−1355

are lengthening of the anhydride ring C−O_b bond and shortening of the MeO−C and C═O_a bonds in the latter. This combination of destabilizing and stabilizing changes possibly results in the nearly isoenergetic relationship between **S-major-IM1** and **S-major TS-2**.

We next examined the corresponding concerted and stepwise pathways to the minor enantiomer in ether. We succeeded in identifying all of the TSs and intermediates, with the exception of the second transition state (**S-minor-TS2**) in the stepwise pathway. It is likely that, analogous to the stepwise pathway leading to the major enantiomer, **S-minor-TS2** is close in energy to **S-minor-IM1**. In their calculations of this ASD reaction with catalysts **II**[36] and **IV**,[33] Aviyente and co-workers also found that the second TS in the stepwise pathway is close in energy to the tetrahedral intermediate (i.e., within 1 kcal/mol) and not rate limiting. Thus, we believe that the first transition states in both the stepwise (**S-minor-TS1**) and concerted (**C-minor-TS1**) pathways leading to the minor enantiomer are rate limiting.

The barriers for all four pathways in diethyl ether—stepwise and concerted leading to **2** and *ent*-**2**—are listed in Table 1.

Table 1. Reaction Barriers[a] for Stepwise and Concerted Pathways Leading to 2 and *ent*-2

entry	product	pathway	$\Delta G^{\ddagger}$ (kcal/mol)
1	**2** (major)	stepwise	17.6
2	*ent*-**2** (minor)	stepwise	20.3
3	*ent*-**2** (minor)	concerted	20.9
4	**2** (major)	concerted	27.9

[a]B3LYP-GD3BJ/6-31+G(d,p)//B3LYP/6-31G(d); calculations performed using SMD implicit diethyl ether solvent.

Interestingly, both stepwise and concerted barriers leading to *ent*-**2** are nearly isoenergetic (entries 2 and 3; $\Delta\Delta G^{\ddagger}$ = 0.6 kcal/mol) and easily surmounted at room temperature. This contrasts with the distinct favorability of the stepwise over the concerted pathway leading to **2** (entry 1 vs 4). The lowest barrier overall is the stepwise pathway leading to the major enantiomer, which is 2.65 kcal/mol lower than the lowest barrier leading to the minor enantiomer. Based on this energy difference, the predicted ee (**2**/*ent*-**2**) is 98%, in excellent agreement with the observed ee of 96%.[15]

The fact that we compute the ee with such accuracy is in contrast to the DFT studies by Aviyente and co-workers mentioned in the introduction.[33] Although they identified transition states and intermediates for both the stepwise and concerted pathways for catalyst **IV** (Figure 2), their calculations predict the favored enantiomer to be opposite to that obtained experimentally. In their case, the free energies of activation for the *concerted* pathways are lower in energy (by about 1 kcal/mol in either the gas phase or toluene solution), whereas we identified the *stepwise* pathways to be lower in energy. Also note that **IV** is significantly less enantioselective than **I** for the substrate that they modeled (ee 72% vs 94%).

The stepwise pathway appears to be only viable for *bifunctional* catalysts, such as **I**, **II**, and **IV**. In their DFT study of catalyst **III** (modeled by compound **V**, Figure 2), which lacks the hydroxyl proton of the native alkaloid, Wong and Yang identified concerted TSs but not stepwise TSs.[37] Thus, the additional stabilization provided by a hydrogen bond donating functional group, β to the quinuclidine nitrogen, appears to enable the tetrahedral intermediate to form. Furthermore, the stepwise pathways are generally lower energy than the concerted pathways for catalysts **I** and **II**; Aviyente and co-workers did not locate a concerted TS for **II**.[36]

Rate-Limiting Transition State Structures. The four rate limiting TS structures are shown in Figure 8, which includes

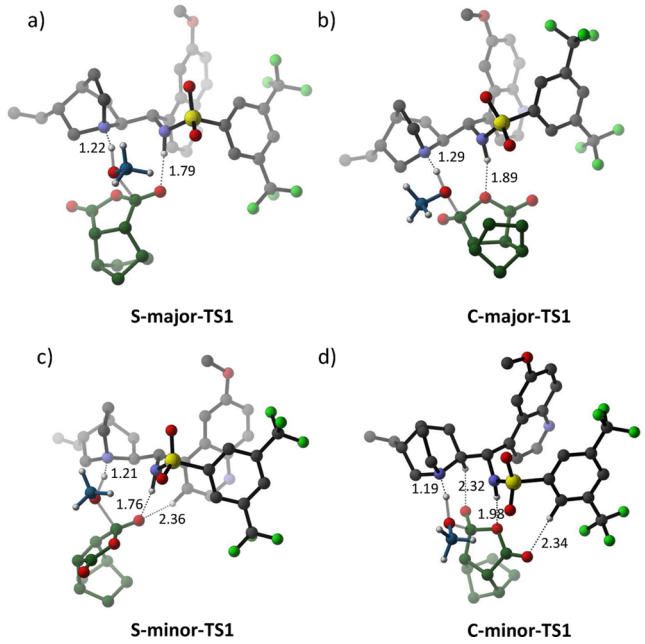

Figure 8. Rate limiting TS structures for stepwise (a) and concerted (b) pathways to **2** and stepwise (c) and concerted (d) pathways to *ent*-**2**, with significant catalyst−reactant complex interactions noted in Å.

significant catalyst−reactant complex interaction distances. Internuclear distances (i = MeOH−NR^*_3) and (ii = O_a−$HNSO_2Ar$) are also listed in Table 2 (columns 2 and 3, respectively), along with other important bond distances. In all of these TSs, the quinuclidine nitrogen acts as general base, consistent with experimental mechanistic data.

As expected for a general base catalyzed mechanism, the most significant bond breaking and bond forming that takes place in all of the rate limiting TSs involves proton transfer from the methanol nucleophile to the quinuclidine nitrogen. Except for the unfavorable **C-major-TS1**, the methanol O−H (1.31−1.34 Å; Table 2, column 1) and quinuclidine N−H (1.19−1.22 Å; Table 1, column 2) distances indicate a degree of proton transfer that has progressed beyond an idealized symmetrical transition state. These bond distances differ dramatically from those identified by Song and co-workers (relevant distances: O−H = 1.00 Å, N−H = 1.71 Å), which underscores the importance of doing a complete DFT TS search as opposed to using molecular mechanics to find minimum energy structures of transition state analogs. The other important bond forming that occurs in the transition state is between the methanol oxygen and the carbonyl carbon, which becomes tetrahedral (Table 2, column 5).

This bifunctional catalyst (**I**) was designed to use the sulfonamide proton to stabilize negative charge in the transition state. Indeed, all of the transition states show close interactions between an oxygen atom on the tetrahedral carbon of the substrate and the sulfonamide proton of the catalyst. The substrate-O to H-sulfonamide distances range from 1.76 to 1.98 Å, with the strongest interactions taking place in the stepwise pathways (Table 2, column 3). The carbonyl oxygen (O_a,

DOI: 10.1021/acs.joc.6b02320
J. Org. Chem. 2017, 82, 1347−1355

Table 2. Distances in Calculated First Transition States[a]

		1	2	3	4	5	6	7
		MeO−H−NR*$_3$		O−H−NSO$_2$Ar		Tetrahedral C		
entry		O−H	N−H (i)	O−H (ii)	N−H	C-OMe	C=O$_a$	C−O$_b$
1	**S-major-TS1**	*1.31*	1.22	1.79[b]	1.04	1.94	1.23	1.45
2	**S-minor-TS1**	*1.33*	1.21	1.76[b]	1.04	1.89	1.24	1.44
3	**C-minor-TS1**	*1.34*	1.19	1.98[c]	1.02	1.94	1.22	*1.49*
4	**C-major-TS1**	*1.25*	1.29	1.89[c]	1.02	1.85	1.22	*1.54*

[a]Distances are in Å. [b]Distance to the carbonyl oxygen (O$_a$) of **3** or *ent*-**3**. [c]Distance to the oxygen in the anhydride ring (O$_b$) of **3** or *ent*-**3**. Distances corresponding to bonds that are breaking are in italics while those of bonds that are forming are underlined.

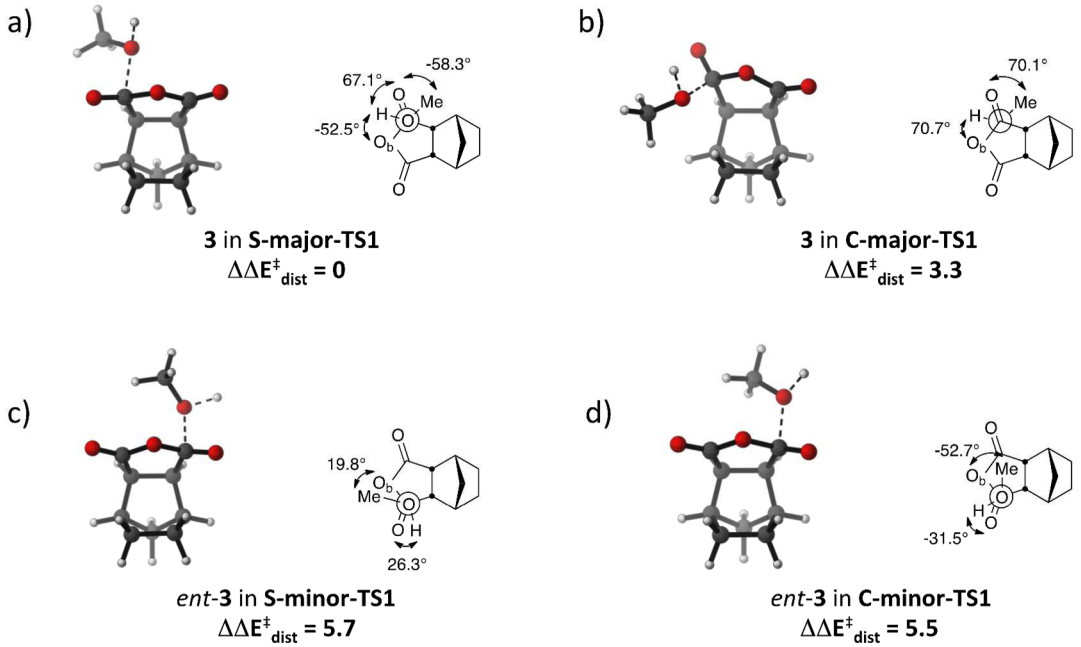

Figure 9. Structures and Newman projections of the reactant complexes leading to **2** (a, b) and *ent*-**2** (c, d) in the four TS complexes, including $\Delta\Delta E^{\ddagger}_{dist}$ energies in kcal/mol (relative to **3** in **S-major-TS1**).

Figure 6) is stabilized in the stepwise mechanisms, whereas the anhydride ring oxygen (O$_b$, Figure 6) is stabilized in the concerted processes. While the C=O$_a$ bond distances between stepwise and concerted pathways are similar (Table 2, column 6), the C−O$_b$ (anhydride) bond lengths are greater in the concerted pathways (Table 2, column 7). This is consistent with the sulfonamide-H···O$_b$ interaction and increased bond breaking at this location in the concerted TSs. Note that we saw no evidence of transition states in which the catalyst sulfonamide proton hydrogen bonds to the *opposite* carbonyl oxygen (O$_c$, Figure 6), as has been identified for native cinchona alkaloid catalysts, such as **II**.[35]

The approach of methanol to the anhydride substrate differs among the calculated transition states in several ways (Figure 9). Methanol attacks the less hindered face of the anhydride (opposite to the bicyclic ring substituent) in all cases except the concerted transition state leading to the major enantiomer, in which it attacks the more congested face (Figure 9b). The methyl substituent of the nucleophile is outside the anhydride ring in both transition states leading to the major enantiomer, with H$_3$C−O−C−O$_b$ dihedral angles of −178° for the stepwise and −172° for the concerted mechanism (Figure 9a,b), corresponding to an *anti* relationship with the anhydride oxygen. In contrast, the methyl substituent is nearly eclipsed (Figure 9c) or gauche (Figure 9d) to the anhydride oxygen (O$_b$) in the transition states leading to the minor enantiomer. Importantly, the complexes leading to **2** and *ent*-**2** are not mirror images of one another; in the presence of catalyst **I**, these complexes adopt diastereomeric conformations.

The apparent strain in the conformers adopted by *ent*-**3** (Figure 9c, d), relative to the conformer adopted by **3** for the stepwise pathway (Figure 9a), prompted us to evaluate their differences in energy. We used the distortion versus interaction (or activation versus strain)[60−63] model for evaluating the rate limiting transition states, in order to separate the energy due to distortion of catalyst **I** and reactants that form species **3** (or *ent*-**3**) from the energy of interaction between catalyst **I** and **3** (or *ent*-**3**). In our analysis, $\Delta E^{\ddagger} = \Delta E^{\ddagger}_{dist}(\mathbf{I}) + \Delta E^{\ddagger}_{dist}(\mathbf{3}\text{ or }ent\text{-}\mathbf{3}) + \Delta E^{\ddagger}_{int}$, where $\Delta E^{\ddagger}_{dist}$ is the strain of **I**, **3**, or *ent*-**3** in the TS, relative to the free species, and $\Delta E^{\ddagger}_{int}$ is the energy of the catalyst−reactant interaction. $\Delta E^{\ddagger}_{dist}(\mathbf{I})$ was calculated by deleting the atoms representing **3** (or *ent*-**3**) from the TS, calculating the single-point energy (B3LYP-GD3BJ/6-31+G-(d,p) SMD implicit diethyl ether) of the catalyst portion of the TS by itself, and subtracting the energy of the free catalyst. Distortion values for **3** or *ent*-**3** were performed in an analogous way, in which the single-point energy of **3** or *ent*-**3** in the TS was compared with the sum of the energies of free **1** and methanol. The $\Delta E^{\ddagger}_{int}$ values were then determined by subtracting the distortion energies from $\Delta E^{\ddagger}$. The similarities

DOI: 10.1021/acs.joc.6b02320
J. Org. Chem. 2017, 82, 1347−1355

in MeO−H and C−OMe bond distances among the three most energetically relevant species (**S-major-TS1**, **S-minor-TS1**, and **C-minor-TS1**: Table 2, columns 1, 5) suggest that the position of the three TSs along their respective reaction coordinates is comparable—none of these three TSs is particularly earlier or later than the others. Thus, for these three species, it is reasonable to compare the energies of distortion and interaction at the TS in this way.

*The values in Table 3 indicate that substantially increased distortion of ent-***3** *(entries 2, 3), relative to* **3** *(entry 1), is the primary factor responsible for enantioselectivity in this transformation.* The catalyst conformers are very similar among the TSs, as evidenced by distortion energies of **I** that differ by only 1 kcal/mol. The interaction energies are slightly stronger for the TSs leading to the minor enantiomer, although that relative stabilization is overwhelmed by the significantly worse distortion energies for *ent*-**3**.

Table 3. Distortion versus Interaction Energies[a] for Rate Limiting Transition States

entry	transition state	$\Delta G^{\ddagger}$	$\Delta E^{\ddagger}$	$\Delta E^{\ddagger}_{dist}$ (**I**)[b]	$\Delta E^{\ddagger}_{dist}$ (**3** or *ent*-**3**)[c]	$\Delta E^{\ddagger}_{int}$[d]
1	**S-major-TS1**	17.6	−11.2	5.4	44.9	−61.4
2	**S-minor-TS1**	20.3	−7.6	4.4	50.6	−62.7
3	**C-minor-TS1**	20.9	−7.5	5.4	50.4	−63.3
4	**C-major-TS1**	27.9	−0.7	4.3	48.2	−53.3

[a]B3LYP-GD3BJ/6-31+G(d,p)//B3LYP/6-31G(d) in kcal/mol. [b]Calculated by performing single-point calculations of the catalyst portion of the TS (B3LYP-GD3BJ/6-31+G(d,p) with SMD implicit diethyl ether) and subtracting the single-point energy of the free catalyst. [c]Calculated by performing single-point calculations of the reactant portion of the TS (**3** or *ent*-**3**; B3LYP-GD3BJ/6-31+G(d,p) with SMD implicit diethyl ether) and subtracting the energies of free **1** and methanol. [d]Calculated from this equation: $\Delta E^{\ddagger} = \Delta E^{\ddagger}_{dist}(\mathbf{I}) + \Delta E^{\ddagger}_{dist}(\mathbf{3}\text{ or }ent\text{-}\mathbf{3}) + \Delta E^{\ddagger}_{int}$.

The increased distortion energy of *ent*-**3** in the stepwise pathway largely arises from partially eclipsing bonds (Figure 9c). For *ent*-**3** in the concerted pathway, a less staggered conformer and steric interactions between methanol and both ring juncture hydrogens combine to destabilize **C-minor-TS1** relative to **S-major-TS1** (Figure 9d). Analogous interactions also could explain the improved selectivity that is observed when more hindered nucleophiles, such as benzyl alcohol[21] and cyclohexyl mercaptan,[64] are used in the organocatalytic ASD with less selective substrates, glutaric anhydrides. In these cases, the minor enantiomer would be disfavored to a greater extent by pseudo 1,3-diaxial interactions between the larger nucleophile and a pseudo axial proton in the glutaric anhydride ring. The strain would not be as significant for the TS that yields the major enantiomer because the nucleophile substituent is oriented away from the ring in that TS.

The catalyst structures in all four TSs are virtually identical; in particular, the quinuclidine and sulfonamide moieties that interact with the reactants are unchanged. The additional catalyst distortion in entries 1 and 3 (Table 3) arises from rotation around the O_2S−Ar (Ar = 3,5$(CF_3)_2$Ph) bond by about 10°, which leads to slightly reduced π stacking in the structures of **I**. The O_2S−Ar bond rotation is correlated with the position of the carbonyl oxygen (O_a) in the stepwise pathways or the anhydride oxygen (O_b) in the concerted pathways, relative to the sulfonamide NH to which they hydrogen bond. For example, a comparison of **3** in **S-major-TS1** (Figure 9a) and *ent*-**3** in **S-minor-TS1** (Figure 9c) shows a significantly greater H−O−C═O dihedral angle in the former (67.1° vs 26.3°), which positions O_a closer to the Ar substituent. However, it is not immediately obvious how the different spatial position of O_a induces the catalyst distortion.

The interaction energy differences among entries 1−3 (Table 3) are also small compared to the differences in distortion energies. The more favorable interaction energy calculated for **S-minor-TS1** (entry 2) than for **S-major-TS1** (entry 1) is likely due to slightly stronger interactions (i) and (ii) in the former (Table 2, columns 2, 3), and possibly also from better 6′-methoxyquinoline (Ar′) $C_3H\cdots O_a$ hydrogen bonding. Similar CH···O hydrogen bonding has been of demonstrated importance for generating an oxyanion hole in model compound **V**, used in the study of catalyst **III**.[37] The species **S-minor-TS1** shows a closer interaction between these groups (Ar′H···O_a = 2.4 Å; distance (iii) in Figure 8c) than **S-major-TS1** (Ar′H···O_a = 2.7 Å). The additional stabilization of **C-minor-TS1** relative to **S-major-TS1** may be due to additional catalyst CH hydrogen bonding interactions with O_a and O_c (distances iv and v, Figure 8d).

The distortion−interaction calculations for **C-major-TS1** show a considerably weaker interaction energy, compared with the other TSs. Bond distances (Table 2, columns 1, 2) indicate that **I** is not as competent a base in this TS (entry 4), compared with the other TSs. The shorter C−OMe bond distance (Table 2, column 5), accompanied by greater tetrahedral character at the carbon undergoing nucleophilic attack (Figure 9b), indicate that this TS falls significantly later than the others along the reaction coordinate. The interaction energy would normally be stronger (more negative) for a later TS;[63] the fact that it is weaker in **C-major-TS1** makes it safe to conclude that the dominant reason why this pathway is not favored is because **I** performs poorly at stabilizing species **3** in the concerted mechanism.

Our results highlight the importance of exploring the spatial relationship between anhydride and methanol (the reactants) *in the course of identifying the diastereomeric TSs with the catalyst of interest.* Otherwise, we would not have recognized that the more distorted conformers of *ent*-**3** in **S-minor-TS1** and **C-minor-TS1**, compared with the conformer of **3** in **S-major-TS1**, would lead to reasonably low energy TSs and the dominant pathways to the minor enantiomer. Also noteworthy in this regard is the ability of stronger interaction energies to overcome, at least in part, the increased distortion energies of what at first appear to be very unfavorable reactant conformers. The previous DFT studies of succinic anhydride desymmetrization using catalysts **II**,[36] **III** (via model compound **V**),[37] and **IV**[33] in this ASD transformation utilize enantiomeric conformations of the anhydride−methanol complex to locate the TSs with chiral catalysts. In all of these previous studies, the conformations are analogous to the structure of **3** in **S-major-TS1** (Figure 9a) and its mirror image. To identify this conformer, Yang and Wong explored the reactant conformational space with *achiral* model catalysts.[37] Because the presence of a *chiral* catalyst creates diastereomeric complexes with these conformers, it is possible that the thus-identified conformer may no longer be the lowest energy for at least one of the enantiomers. In other words, it cannot be assumed that the conformers of the reactant complexes leading to each enantiomer will have a mirror image relationship to one another in the chiral catalyst−reactant complex.

DOI: 10.1021/acs.joc.6b02320
J. Org. Chem. 2017, 82, 1347−1355

CONCLUSIONS

In conclusion, we have identified rate limiting TSs for both stepwise and concerted pathways to desymmetrize cyclic anhydride **1** using a methanol nucleophile and sulfonamide-derivitized cinchona alkaloid catalyst **I** in diethyl ether. The stepwise pathway leading to the major enantiomer is significantly favored over the concerted pathway, whereas the concerted and stepwise rate limiting TSs leading to the minor enantiomer are nearly isoenergetic.

All four TSs are consistent with a general base role for the quinuclidine moiety of catalyst **I**. We identified two important hydrogen bonding interactions in the transition states: (i) between the catalyst quinuclidine moiety and the methanol hydroxyl proton and (ii) between the catalyst sulfonamide proton and an oxygen atom attached to the carbonyl carbon of the substrate, which becomes pyramidal in the TSs. Of the four identified reaction barriers, three are energetically accessible at room temperature. The lowest two predict an ee of 98% in favor of the major enantiomer, in excellent agreement with the experimental ee of 96%. Distortion versus interaction calculations indicate that increased distortion energies for the anhydride−methanol complex (*ent*-**3**) in the TS structures leading to the minor enantiomer, relative to those in the complex (**3**) leading to the major enantiomer, are primarily responsible for the enantioselectivity of this reaction. The increased distortion is largely due to torsional and steric strain in conformers of *ent*-**3**. The increased strain between the nucleophile and anhydride ring in the TS leading to the minor enantiomer provides a rationale for why larger nucleophiles lead to greater enantioselectivity in the ASD of cyclic glutaric anhydrides.[21,64] Future investigations will focus on the interplay between the nucleophile and anhydride for controlling the enantioselectivity of this transformation with additional substrates.

EXPERIMENTAL SECTION

Compound **I** was prepared according to the literature procedure.[19] COSY and NOESY ^{1}H NMR spectra were acquired at 400 or 500 MHz in $CDCl_3$ and 400 MHz in Et_2O-d_{10}, and spectra were referenced to residual $CHCl_3$ (7.26 ppm) or Et_2O-d_9 (1.07 or 3.34 ppm).

Geometry optimizations and transition state searches using density functional theory (B3LYP-GD3BJ/6-31+G(d,p)//B3LYP/6-31G(d)), in implicit diethyl ether or chloroform solvent (SMD),[59] were used to study catalyst **I** and to perform mechanistic studies of the reaction in eq 1. Intermediates and transition states for both stepwise and concerted pathways to produce the major enantiomer were located and confirmed with frequency analyses and intrinsic reaction coordinate calculations. The analogous TSs for the rate-determining steps to produce the minor enantiomer were located in a similar fashion. All calculations were performed using the Gaussian 09 computational package.[65]

ASSOCIATED CONTENT

Supporting Information

The Supporting Information is available free of charge on the ACS Publications website at DOI: 10.1021/acs.joc.6b02320.

Optimized geometries energies, functional and catalyst conformer comparison (PDF)

Spectral data (PDF)

Cartesian coordinates of stationary points (ZIP)

AUTHOR INFORMATION

Corresponding Authors

*E-mail: ghofmeis@carleton.edu.

*E-mail: dkohen@carleton.edu.

ORCID

Gretchen E. Hofmeister: 0000-0002-7858-2528

Daniela Kohen: 0000-0001-7900-1660

Notes

The authors declare no competing financial interest.

ACKNOWLEDGMENTS

This work was supported by Carleton College through funding from the Howard Hughes Medical Institute Undergraduate Science Education Grant and the Harry A. and Margaret D. Towsley Foundation Fellowships in the Sciences as well as the National Science Foundation under CHE-1039925 (for computing resources) and CHE-1428752 (for the NMR spectrometer). We are grateful to Keith Kuwata (Macalester College), David Alberg, and Buck Taylor (both of Carleton College) for providing helpful comments. David Alberg obtained 2D NMR spectra in Et_2O-d_{10}. Alex Lai prepared the didehydro analog of hemiester **2**. Letitia Yao (University of Minnesota) obtained NMR data at 500 MHz in $CDCl_3$.

REFERENCES

(1) Spivey, A. C.; Andrews, B. I. *Angew. Chem., Int. Ed.* **2001**, *40*, 3131−3134.

(2) Chen, Y.; McDaid, P.; Deng, L. *Chem. Rev.* **2003**, *103*, 2965−2983.

(3) Atodiresei, I.; Schiffers, I.; Bolm, C. *Chem. Rev.* **2007**, *107*, 5683−5712.

(4) Spivey, A. C.; McDaid, P. In *Enantioselective Organocatalysis*; Dalko, P. I., Ed.; Wiley-VCH Verlag GmbH & Co.: Weinheim, 2007; pp 287−329.

(5) Borissov, A.; Davies, T. Q.; Ellis, S. R.; Fleming, T. A.; Richardson, M. S. W.; Dixon, D. J. *Chem. Soc. Rev.* **2016**, *45*, 5474−5540.

(6) Hamersak, Z.; Stipetic, I.; Avdagic, A. *Tetrahedron: Asymmetry* **2007**, *18*, 1481−1485.

(7) Xiong, F.; Chen, X.-X.; Chen, F.-E. *Tetrahedron: Asymmetry* **2010**, *21*, 665−669.

(8) Diaz de Villegas, M. D.; Galvez, J. A.; Etayo, P.; Badorrey, R.; Lopez-Ram-de-Viu, P. *Chem. Soc. Rev.* **2011**, *40*, 5564−5587.

(9) Sakai, M.; Ishikawa, Y.; Takamizawa, S.; Oikawa, M. *Tetrahedron Lett.* **2013**, *54*, 5911−5912.

(10) Sakai, M.; Tanaka, K.; Takamizawa, S.; Oikawa, M. *Tetrahedron* **2014**, *70*, 4587−4594.

(11) Nagatomo, M.; Hagiwara, K.; Masuda, K.; Koshimizu, M.; Kawamata, T.; Matsui, Y.; Urabe, D.; Inoue, M. *Chem. - Eur. J.* **2016**, *22*, 222−229.

(12) Chen, Y.; Tian, S.-K.; Deng, L. *J. Am. Chem. Soc.* **2000**, *122*, 9542−9543.

(13) Connon, S. J. *Chem. Commun.* **2008**, 2499−2510.

(14) Peschiulli, A.; Gun'k, Y.; Connon, S. J. *J. Org. Chem.* **2008**, *73*, 2454−2457.

(15) Rho, H. S.; Oh, S. H.; Lee, J. W.; Lee, J. Y.; Chin, J.; Song, C. E. *Chem. Commun.* **2008**, 1208−1210.

(16) Schmitt, E.; Schiffers, I.; Bolm, C. *Tetrahedron* **2010**, *66*, 6349−6357.

(17) Malerich, J. P.; Hagihara, K.; Rawal, V. H. *J. Am. Chem. Soc.* **2008**, *130*, 14416−14417.

(18) Jang, H. B.; Rho, H. S.; Oh, J. S.; Nam, E. H.; Park, S. E.; Bae, H. Y.; Song, C. E. *Org. Biomol. Chem.* **2010**, *8*, 3918−3922.

(19) Oh, S. H.; Rho, H. S.; Lee, J. W.; Lee, J. E.; Youk, S. H.; Chin, J.; Song, C. E. *Angew. Chem., Int. Ed.* **2008**, *47*, 7872−7875.

DOI: 10.1021/acs.joc.6b02320
J. Org. Chem. 2017, 82, 1347−1355

(20) Bae, H. Y.; Song, C. E. *Bull. Korean Chem. Soc.* **2014**, *35*, 1590−1600.
(21) Park, S. E.; Nam, E. H.; Jang, H. B.; Oh, J. S.; Some, S.; Lee, Y. S.; Song, C. E. *Adv. Synth. Catal.* **2010**, *352*, 2211−2217.
(22) Lu, X.; Deng, L. *Org. Lett.* **2014**, *16*, 2358−2361.
(23) Luo, J.; Xu, L.-W.; Hay, R. A. S.; Lu, Y. *Org. Lett.* **2009**, *11*, 437−440.
(24) Breman, A. C.; Telderman, S. E. M.; van Santen, R. P. M.; Scott, J. I.; van Maarseveen, J. H.; Ingemann, S.; Hiemstra, H. *J. Org. Chem.* **2015**, *80*, 10561−10574.
(25) For a recent review of computational studies of cinchona alkaloid based organocatalysts, see: Tanriver, G.; Dedeoglu, B.; Catak, S.; Aviyente, V. *Acc. Chem. Res.* **2016**, *49*, 1250−1262.
(26) For example, substrate **1** proceeds with 96% ee and the calculated energy difference between the transition states is 4.93 kcal/mol.
(27) Hiratake, J.; Yamamoto, Y.; Oda, J. i. *J. Chem. Soc., Chem. Commun.* **1985**, 1717−1719.
(28) Hiratake, J.; Inagaki, M.; Yamamoto, Y.; Oda, J. *J. Chem. Soc., Perkin Trans. 1* **1987**, 1053−1058.
(29) Aitken, R. A.; Gopal, J.; Hirst, J. A. *J. Chem. Soc., Chem. Commun.* **1988**, 632−634.
(30) Bigi, F.; Carloni, S.; Maggi, R.; Mazzacani, A.; Sartori, G.; Tanzi, G. *J. Mol. Catal. A: Chem.* **2002**, *182*−*183*, 533−539.
(31) Li, H. M.; Liu, X. F.; Wu, F. H.; Tang, L. A.; Deng, L. *Proc. Natl. Acad. Sci. U. S. A.* **2010**, *107*, 20625−20629.
(32) Balzano, F.; Jumde, R. P.; Mandoli, A.; Masi, S.; Pini, D.; Uccello-Barretta, G. *Chirality* **2011**, *23*, 784−795.
(33) Dedeoglu, B.; Catak, S.; Houk, K. N.; Aviyente, V. *ChemCatChem* **2010**, *2*, 1122−1129.
(34) Bolm, C.; Schiffers, I.; Dinter, C. L.; Gerlach, A. *J. Org. Chem.* **2000**, *65*, 6984−6991.
(35) Ivsic, T.; Novak, J.; Doslic, N.; Hamersak, Z. *Tetrahedron* **2012**, *68*, 8311−8317.
(36) Dedeoglu, B.; Catak, S.; Yildirim, A.; Bolm, C.; Aviyente, V. *ChemCatChem* **2015**, *7*, 4173−4179.
(37) Yang, H.; Wong, M. W. *J. Am. Chem. Soc.* **2013**, *135*, 5808−5818.
(38) Silva, T. H. A.; Oliveira, A. B.; De Almeida, W. B. *Struct. Chem.* **1997**, *8*, 95−107.
(39) Silva, T. H. A.; Oliveira, A. B.; De Almeida, W. B. *Bioorg. Med. Chem.* **1997**, *5*, 353−361.
(40) Burgi, T.; Baiker, A. *J. Am. Chem. Soc.* **1998**, *120*, 12920−12926.
(41) Dijkstra, G. D. H.; Kellogg, R. M.; Wynberg, H. *Recl. Trav. Chim. Pays-Bas* **1989**, *108*, 195−204.
(42) Dijkstra, G. D. H.; Kellogg, R. M.; Wynberg, H.; Svendsen, J. S.; Marko, I.; Sharpless, K. B. *J. Am. Chem. Soc.* **1989**, *111*, 8069−8076.
(43) Dijkstra, G. D. H.; Kellogg, R. M.; Wynberg, H. *J. Org. Chem.* **1990**, *55*, 6121−6131.
(44) Vargas, A.; Bonalumi, N.; Ferri, D.; Baiker, A. *J. Phys. Chem. A* **2006**, *110*, 1118−1127.
(45) Urakawa, A.; Meier, D. M.; Ruegger, H.; Baiker, A. *J. Phys. Chem. A* **2008**, *112*, 7250−7255.
(46) Busygin, I.; Nieminen, V.; Taskinen, A.; Sinkkonen, J.; Toukoniitty, E.; Sillanpaa, R.; Murzin, D. Y.; Leino, R. *J. Org. Chem.* **2008**, *73*, 6559−6569.
(47) Silva, T. H. A.; Oliveira, A. B.; Dos Santos, H. F.; De Almeida, W. B. *Struct. Chem.* **2001**, *12*, 431−437.
(48) Tarkanyi, G.; Kiraly, P.; Varga, S.; Vakulya, B.; Soos, T. *Chem. - Eur. J.* **2008**, *14*, 6078−6086.
(49) Kiraly, P.; Soos, T.; Varga, S.; Vakulya, B.; Tarkanyi, G. *Magn. Reson. Chem.* **2010**, *48*, 13−19.
(50) Hara, N.; Nakamura, S.; Sano, M.; Tamura, R.; Funahashi, Y.; Shibata, N. *Chem. - Eur. J.* **2012**, *18*, 9276−9280.
(51) Ferri, D.; Burgi, T.; Baiker, A. *J. Chem. Soc., Perkin Trans. 2* **1999**, 1305−1311.
(52) Ferri, D.; Burgi, T.; Baiker, A. *J. Chem. Soc., Perkin Trans. 2* **2002**, 437−441.
(53) Olsen, R. A.; Borchardt, D.; Mink, L.; Agarwal, A.; Mueller, L. J.; Zaera, F. *J. Am. Chem. Soc.* **2006**, *128*, 15594−15595.
(54) Mink, L.; Ma, Z.; Olsen, R. A.; James, J. N.; Sholl, D. S.; Mueller, L. J.; Zaera, F. *Top. Catal.* **2008**, *48*, 120−127.
(55) Grimme, S.; Ehrlich, S.; Goerigk, L. *J. Comput. Chem.* **2011**, *32*, 1456−1465.
(56) Kacprzak, K.; Gierczyk, B. *Tetrahedron: Asymmetry* **2010**, *21*, 2740−2745.
(57) Cheong, P. H. Y.; Legault, C. Y.; Um, J. M.; Celebi-Olcum, N.; Houk, K. N. *Chem. Rev.* **2011**, *111*, 5042−5137.
(58) http://www.ccdc.cam.ac.uk/.
(59) Marenich, A. V.; Cramer, C. J.; Truhlar, D. G. *J. Phys. Chem. B* **2009**, *113*, 6378−6396.
(60) Bickelhaupt, F. M. *J. Comput. Chem.* **1999**, *20*, 114−128.
(61) Ess, D. H.; Houk, K. N. *J. Am. Chem. Soc.* **2007**, *129*, 10646−10647.
(62) Ess, D. H.; Houk, K. N. *J. Am. Chem. Soc.* **2008**, *130*, 10187−10198.
(63) Fernandez, I.; Bickelhaupt, F. M. *Chem. Soc. Rev.* **2014**, *43*, 4953−4967.
(64) Peschiulli, A.; Quigley, C.; Tallon, S.; Gun'ko, Y. K.; Connon, S. J. *J. Org. Chem.* **2008**, *73*, 6409−6412.
(65) Frisch, M. J.; Trucks, G. W.; Schlegel, H. B.; Scuseria, G. E.; Robb, M. A.; Cheeseman, J. R.; Scalmani, G.; Barone, V.; Mennucci, B.; Petersson, G. A.; Nakatsuji, H.; Caricato, M.; Li, X.; Hratchian, H. P.; Izmaylov, A. F.; Bloino, J.; Zheng, G.; Sonnenberg, J. L.; Hada, M.; Ehara, M.; Toyota, K.; Fukuda, R.; Hasegawa, J.; Ishida, M.; Nakajima, T.; Honda, Y.; Kitao, O.; Nakai, H.; Vreven, T.; Montgomery, J. A., Jr.; Peralta, J. E.; Ogliaro, F.; Bearpark, M. J.; Heyd, J.; Brothers, E. N.; Kudin, K. N.; Staroverov, V. N.; Kobayashi, R.; Normand, J.; Raghavachari, K.; Rendell, A. P.; Burant, J. C.; Iyengar, S. S.; Tomasi, J.; Cossi, M.; Rega, N.; Millam, N. J.; Klene, M.; Knox, J. E.; Cross, J. B.; Bakken, V.; Adamo, C.; Jaramillo, J.; Gomperts, R.; Stratmann, R. E.; Yazyev, O.; Austin, A. J.; Cammi, R.; Pomelli, C.; Ochterski, J. W.; Martin, R. L.; Morokuma, K.; Zakrzewski, V. G.; Voth, G. A.; Salvador, P.; Dannenberg, J. J.; Dapprich, S.; Daniels, A. D.; Farkas, Ö.; Foresman, J. B.; Ortiz, J. V.; Cioslowski, J.; Fox, D. J. *Gaussian 09*; Gaussian, Inc.: Wallingford, CT, USA, 2009.

DOI: 10.1021/acs.joc.6b02320
J. Org. Chem. 2017, 82, 1347−1355